Since January 2020 Elsevier has created a COVID-19 resource centre with free information in English and Mandarin on the novel coronavirus COVID-19. The COVID-19 resource centre is hosted on Elsevier Connect, the company's public news and information website.

Cell Reports

Article

Ablation of Adar1 in myeloid cells imprints a global antiviral state in the lung and heightens early immunity against SARS-CoV-2

Graphical abstract

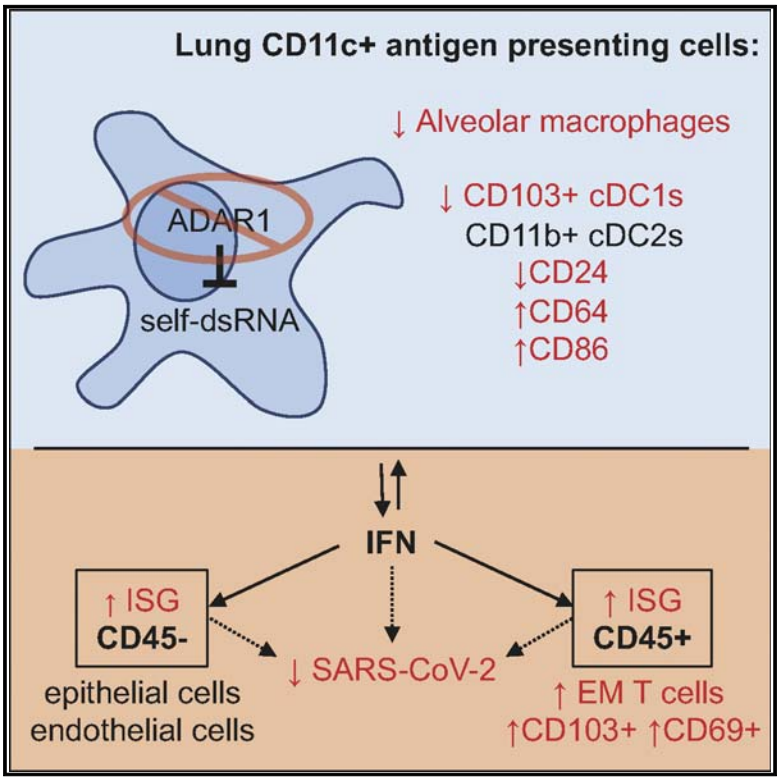

Highlights

- ADAR1 loss in CD11c+ APCs leads to accumulation of inflammatory cDC2-like cells
- ADAR1 loss in APCs imprints an antiviral gene signature in bystander cells
- IFNAR1 blockade partially reverses changes that result from ADAR1 loss in APCs
- ADAR1 loss in APCs promotes early resistance against SARS-CoV-2 infection

Authors

Julia Z. Adamska, Rohit Verma, Shakti Gupta, ..., Mehul S. Suthar, Jin Billy Li, Bali Pulendran

Correspondence

bpulend@stanford.edu

In brief

Adamska et al. show that loss of the RNA-editing enzyme ADAR1 in CD11c+ APCs leads to an accumulation of inflammatory cDC2-like cells. Loss of ADAR1 in APCs further imprints a functional antiviral gene signature in bystander immune and non-immune cells that promotes early resistance against SARS-CoV-2 infection.

Adamska et al., 2023, Cell Reports *42*, 112038
January 31, 2023
https://doi.org/10.1016/j.celrep.2023.112038

CellPress

Cell Reports

CellPress
OPEN ACCESS

Article

Ablation of Adar1 in myeloid cells imprints a global antiviral state in the lung and heightens early immunity against SARS-CoV-2

Julia Z. Adamska,[1,2,12] Rohit Verma,[1,12] Shakti Gupta,[3] Thomas Hagan,[4,5] Florian Wimmers,[1] Katharine Floyd,[9] Qin Li,[2] Erika V. Valore,[1] Yanli Wang,[1] Meera Trisal,[1] José G. Vilches-Moure,[6] Shankar Subramaniam,[3] Carl R. Walkley,[7,8] Mehul S. Suthar,[9] Jin Billy Li,[3] and Bali Pulendran[1,10,11,13,*]

[1]Institute for Immunity, Transplantation and Infection, Stanford University School of Medicine, Stanford University, Stanford, CA 94304, USA
[2]Department of Genetics, Stanford University, Stanford, CA 94305, USA
[3]Department of Bioengineering, University of California, San Diego, San Diego, CA 92093, USA
[4]Division of Infectious Diseases, Cincinnati Children's Hospital Medical Center, Cincinnati, OH 45229, USA
[5]Department of Pediatrics, University of Cincinnati College of Medicine, Cincinnati, OH 45267, USA
[6]Department of Comparative Medicine, Stanford University, Stanford, CA 94305, USA
[7]St. Vincent's Institute of Medical Research, Fitzroy, VIC 3065, Australia
[8]Department of Medicine, St. Vincent's Hospital, University of Melbourne, Fitzroy, VIC 3065, Australia
[9]Department of Pediatrics, Department of Microbiology and Immunology, Emory Vaccine Center, Emory National Primate Center, Emory School of Medicine, Atlanta, GA 30329, USA
[10]Department of Pathology, Stanford University, Stanford, CA 94305, USA
[11]Department of Microbiology & Immunology, Stanford University, Stanford, CA 94305, USA
[12]These authors contributed equally
[13]Lead contact
*Correspondence: bpulend@stanford.edu
https://doi.org/10.1016/j.celrep.2023.112038

SUMMARY

Under normal homeostatic conditions, self-double-stranded RNA (self-dsRNA) is modified by adenosine deaminase acting on RNA 1 (ADAR1) to prevent the induction of a type I interferon-mediated inflammatory cascade. Antigen-presenting cells (APCs) sense pathogen-associated molecular patterns, such as dsRNA, to activate the immune response. The impact of ADAR1 on the function of APCs and the consequences to immunity are poorly understood. Here, we show that ADAR1 deletion in CD11c+ APCs leads to (1) a skewed myeloid cell compartment enriched in inflammatory cDC2-like cells, (2) enhanced numbers of activated tissue resident memory T cells in the lung, and (3) the imprinting of a broad antiviral transcriptional signature across both immune and non-immune cells. The resulting changes can be partially reversed by blocking IFNAR1 signaling and promote early resistance against severe acute respiratory syndrome coronavirus 2 (SARS-CoV-2) infection. Our study provides insight into the consequences of self-dsRNA sensing in APCs on the immune system.

INTRODUCTION

Prompt response against pathogens rests on the capacity of the immune system to respond to a variety of conserved pathogen-associated molecular patterns (PAMPs) through pattern-recognition receptors (PRRs). Long double-stranded RNA (dsRNA) is one such PAMP, recognized in the cytosol by melanoma differentiation-associated protein 5 (MDA5) and protein kinase R (PKR) to trigger a type 1 interferon (IFN)-mediated inflammatory response and translational shutdown, respectively.[1,2] This paradigm is complicated by the observation that dsRNA also arises as a normal byproduct of the transcription of inverted repetitive elements scattered throughout the genome. Adenosine deaminase acting on RNA 1 (ADAR1) edits self-dsRNA to prevent recognition by PRRs.[3] ADAR1, found as the constitutively expressed p110 isoform in the nucleus and the IFN-inducible p150 isoform in the cytosol, edits adenosine to inosine (A-to-I) in dsRNA to decrease its capacity to serve as a ligand for cytoplasmic dsRNA sensors. ADAR1 is implicated in human diseases. Loss-of-function mutations in ADAR1 result in Aicardi-Goutières syndrome, an inflammatory disorder that manifests through severe encephalopathy with additional systemic lupus erythematosus-like symptoms.[4] Furthermore, dysfunction in ADAR1 expression and editing activity is beginning to be described in a range of inflammatory diseases and cancers.[5]

After physical barriers, innate immune cells represent the first line of defense against pathogens. Antigen-presenting cells (APCs) are endowed with an array of PRRs that enable them to sense diverse PAMPs. Despite evidence that ADAR1 is an important regulator of immunity, the contribution of ADAR1 to

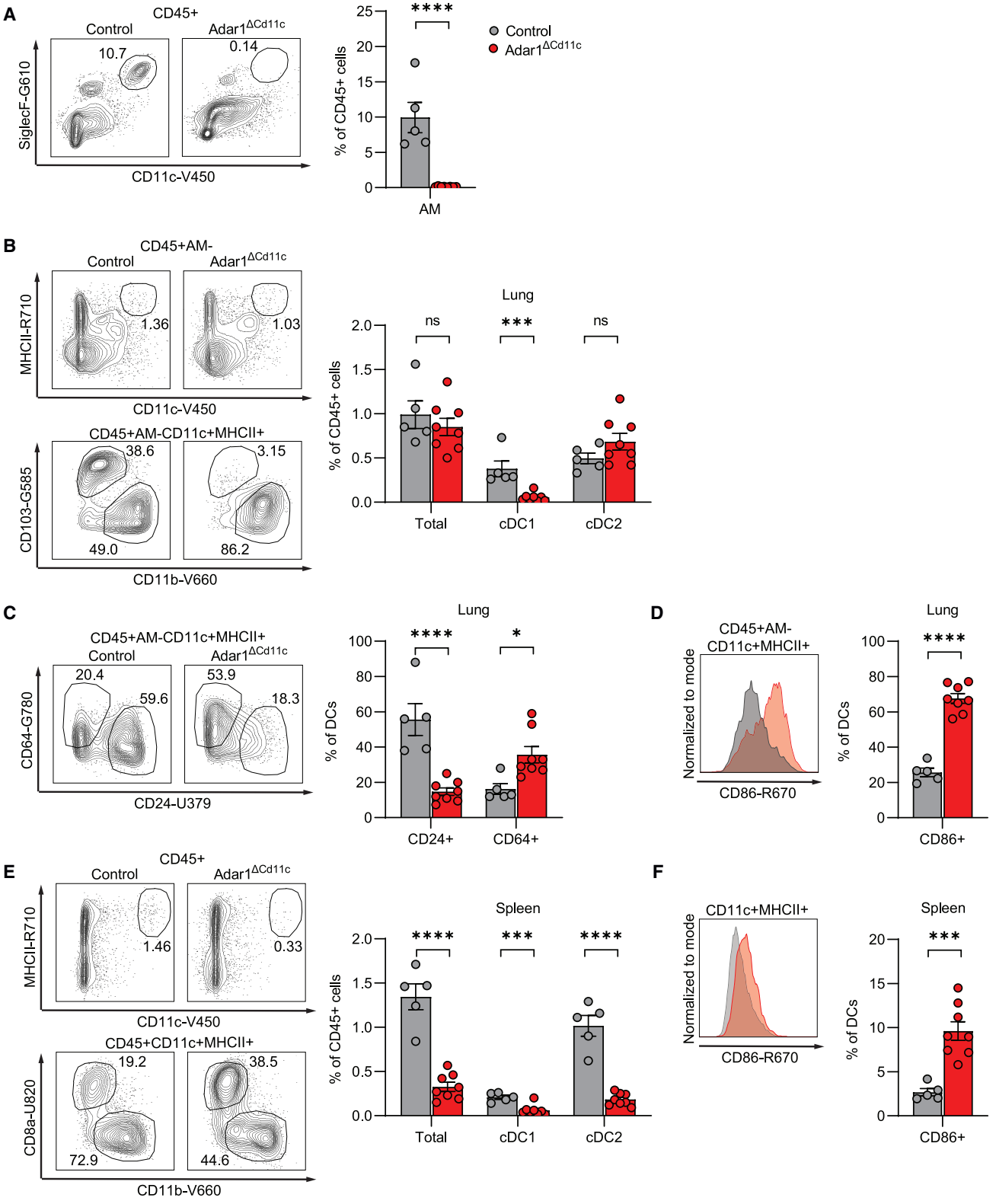

(legend on next page)

the initiation and perpetuation of the immune response is only beginning to be characterized. A previous report demonstrated that genetic deletion of ADAR1 from CD11c-expressing cells resulted in the systemic reduction of CD8α+/CD103+ conventional dendritic cells (cDC1s) and lung-specific loss of alveolar macrophages (AMs).[6] However, the impact of CD11c+ cell ADAR1 deletion on bystander cells and its functional consequences to immunity were not examined. In the present study, we demonstrate that ablation of ADAR1 in CD11c+ cells results in (1) altered myeloid cell compartment composition, including augmented representation of inflammatory cDC2s (inf-cDC2s); (2) enhanced lung tissue infiltration of activated tissue-resident memory T cells (TRMs); (3) the imprinting of an antiviral transcriptional signature across both CD11c+ cells and bystander cells, including non-immune cells; and (4) heightened resistance to early severe acute respiratory syndrome coronavirus 2 (SARS-CoV-2) infection. Further, the resulting changes can be partially reversed by blocking IFNAR1 signaling. These results demonstrate that ADAR1 ablation in APCs acts in *cis* and *trans* to imprint a functional antiviral state.

RESULTS

ADAR1 ablation in CD11c+ cells alters DC and macrophage homeostasis

To investigate the role of ADAR1 in APCs, we generated a CD11c+ cell-specific ADAR1-deficient mouse line by crossing *CD11c-Cre*$^{+/-}$ with *Adar1*$^{fl/fl}$ *R26*^{YFP} mice (hereafter referred to as *Adar1*$^{\Delta Cd11c}$). We first assessed the impact of ADAR1 deletion on the composition of APCs across lymphoid (spleen) and non-lymphoid (lung) tissues. Consistent with the previous report of ADAR1 deletion in CD11c+ cells, we observed a reduction in lung AMs and CD103+ cDC1s (Figures 1A and 1B).[6] CD11b+ cDC2s were observed at comparable frequencies in the lungs of *Adar1*$^{\Delta Cd11c}$ mice (Figure 1B). However, as lung CD11b+ cDC2s represent a heterogeneous population, we next examined the expression of the canonical DC marker CD24 and the monocyte/macrophage marker CD64 within the population. We found that ablation of ADAR1 in CD11c+ skews the composition of the major histocompatibility complex (MHC) class II+CD11c+ DC population within the lung toward the monocyte/macrophage CD24-CD64+ phenotype (Figure 1C). We next assessed the expression of costimulatory molecule CD86 in lung DCs, observing higher frequency of CD86+ DCs in *Adar1*$^{\Delta Cd11c}$ mice compared with controls (Figure 1D). Consistent with the previous report, analysis of a DC subset in the spleen showed reduced DC frequency in *Adar1*$^{\Delta Cd11c}$ due to the loss of both CD8α+ cDC1s and CD11b+ cDC2s (Figure 1E). Splenic DCs in *Adar1*$^{\Delta Cd11c}$ showed a modest yet significant increase in the expression of CD86 (Figure 1F). Thus, we concluded that ADAR1 deletion in APCs results in distinct tissue- and cell-specific phenotypes.

ADAR1 ablation in CD11c^{+} APCs has a global effect on the transcriptional landscape of the immune system

Given the impact of ADAR1 ablation in APCs on APC homeostasis, we sought to characterize the broader consequences of ADAR1-deficient APCs on the immune system. To this end, we combined the 10x Chromium single-cell RNA sequencing (scRNA-seq) platform with a fluorescence-activated cell sorting (FACS)-based enrichment strategy to uncover minor cell populations such as AMs and DCs (Figure 2A). Uniform manifold approximation and projection (UMAP) and graph-based clustering segregated lung single cells pooled from *Adar1*$^{\Delta Cd11c}$ or control mice into 23 clusters, annotated into different cell types based on previous literature and the ImmGen database (Figure 2B).[7] We next analyzed the transcriptional profile of each cluster in *Adar1*$^{\Delta Cd11c}$ and compared it with the respective cluster in control mice to determine the number of differentially expressed genes (DEGs) for each cluster (Figure 2C). Analysis of myeloid and lymphoid cells showed gene expression changes in most of the cell types. Furthermore, interstitial macrophages (IMs; clusters 19 and 1), AMs (cluster 13), cDC2s (cluster 7), and proliferating cells (cluster 6) exhibited the highest number of DEGs. To better visualize altered transcriptional pathways, DEGs were subjected to enrichment analysis using previously defined blood transcriptomics modules (BTMs).[8] This detected a marked enrichment of innate antiviral response gene signatures, viral sensing signatures including retinoic acid-inducible gene I (RIG-I)-like receptor signaling, and cytosolic DNA sensing pathways in most cells[9] (Figure 2D). Clusters 6, 17, and 19, representing a proliferating cell, red blood cells (RBCs), and MHC class II− IMs, respectively, did not show upregulation of these module (Figure 2D). In addition, BTMs related to antigen presentation, chemokines, and cell cycle and growth arrest were heterogeneously enriched across cell types. CD8 T cell (cluster 8), MHC class II+ IMs (cluster 1), and neutrophils (cluster 15) showed upregulation of the genes of the cell cycle and growth arrest module, whereas the same module was downregulated in cDC1s (cluster 14) and cDC2s (cluster 7) (Figure 2D). Analysis of IFN-stimulated genes (ISGs) like *Irf7*, *Isg15*, and *Zbp1* showed broad upregulation across immune cell types in *Adar1*$^{\Delta Cd11c}$ mice (Figure 2E).

Next, to examine whether ADAR1 ablation induces transcriptional changes beyond the lung, we performed scRNA-seq of splenocytes using a similar cell enrichment strategy as described for lung (Figure S1A). UMAP and graph-based clustering segregated

Figure 1. ADAR1 ablation in APCs alters dendritic cell and macrophage homeostasis

Lungs and spleens from naive *Adar1*$^{\Delta Cd11c}$ (red) or control (gray) mice were analyzed by flow cytometry.

(A and B) Frequency of lung (A) SiglecF+CD11c+ alveolar macrophages or (B) total MHC class II+CD11c+ DCs, CD103+ cDC1s, and CD11b+ cDC2s, with representative contour plots.

(C) Lung DCs were subset based on the expression of CD24 and CD64, with representative contour plots.

(D) Expression of the activation marker CD86 on lung DCs, with representative histograms.

(E) Total spleen MHC class II+CD11c+ DCs, CD8a+ cDC1s, and CD11b+ cDC2s, with representative contour plots.

(F) Expression of the activation marker CD86 on spleen DCs, with representative histograms. Results are representative of 3 independent experiments with n = 5–8 per group each, represented as mean ± SEM. Unpaired t test, ns, not significant, *p ≤ 0.05, **p ≤ 0.01, ***p ≤ 0.001, ****p ≤ 0.0001.

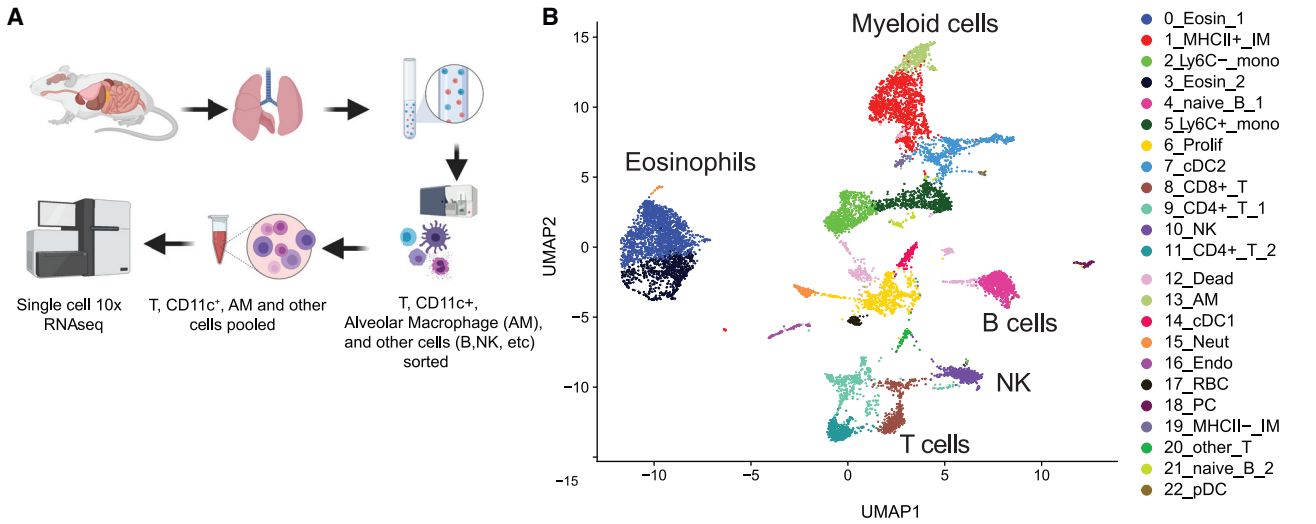

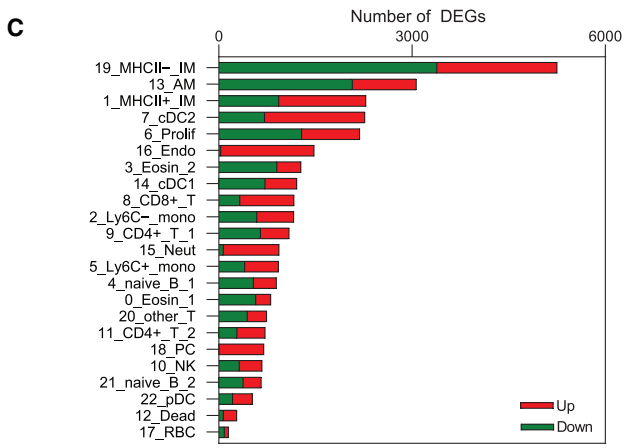

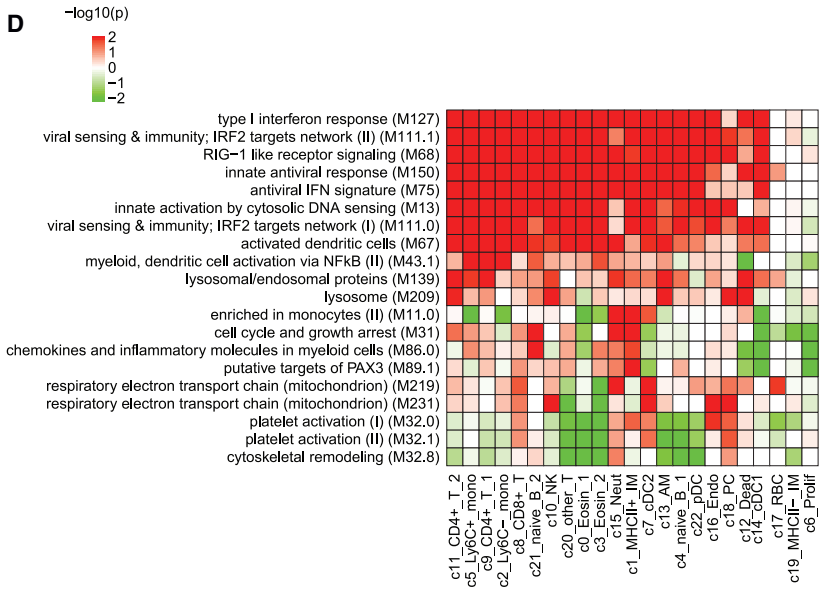

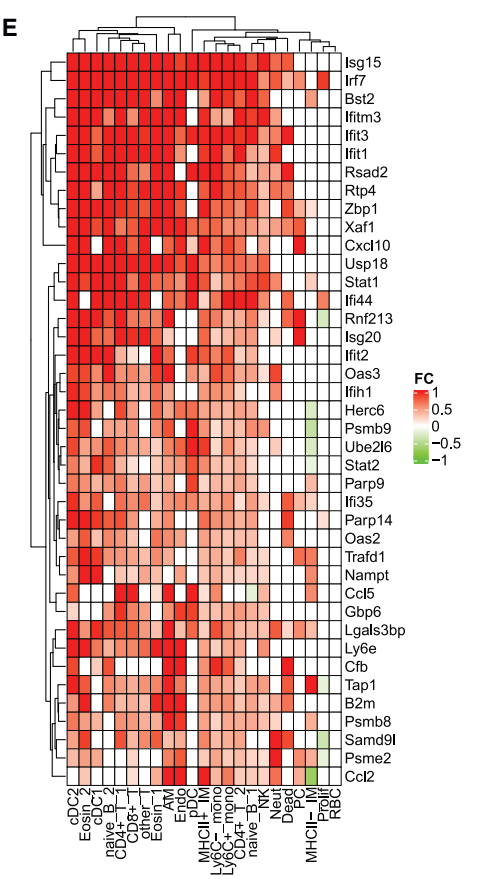

(legend on next page)

spleen single cells pooled from *Adar*$^{\Delta CD11c}$ and control mice into 22 clusters, annotated into different cell types (Figure S1B). Analysis of DEGs showed broad changes in transcriptional profile across different cell types in the spleen (Figure S1C). Neutrophils (clusters 15 and 4), cDC2s (cluster 2), and cDC1s (cluster 11) showed the highest number of DEGs (Figure S1C). Analysis of BTMs in spleen showed upregulation of similar modules as observed in lung, such as innate antiviral response genes, viral sensing signatures, including RIG-I, and cytosolic DNA sensing pathways in most cell clusters, except clusters 5 and 13, which represent macrophage populations (Figure S1D). In the spleen, ADAR1 ablation in APCs showed differential enrichment of BTMs involved with cell cycle, respiratory electron transport chain, and transcriptional activity in myeloid and lymphoid cell clusters. cDC1s, cDC2s, and monocytes showed upregulation of modules of cell cycle, electron transport chain, and transcriptional activity, whereas these modules were not altered in T and B cells (Figure S1D). As in the lungs, analysis of ISGs like *Irf7*, *Isg15*, and *Zbp1* in the spleen showed upregulation across multiple immune cell clusters (Figure S1E). Thus, we conclude that ADAR1 ablation in CD11c+ cells imprints an antiviral transcriptional signature in both APCs and bystander cells across both spleen and lung.

ADAR1 ablation in CD11c$^+$ APCs alters myeloid cell homeostasis and skews the ratio of cDC2s to inflammatory DCs in lungs

To better understand the effect of ADAR1 deficiency in CD11c+ APCs, we separately analyzed the mononuclear phagocyte landscape comprising monocyte, macrophage, and DC clusters in the lungs of *Adar1*$^{\Delta Cd11c}$ and control mice (Figure 3A). To ascertain the identity of monocytes, macrophage, and DCs, we determined the expression of integrin alpha X, encoding CD11c, and master transcription factors *Mafb* and *Zbtb46*, which are differentially expressed in macrophages and DCs, respectively.[10–13] Concordant with literature, we found that CD11c is expressed by DCs, macrophages, and a subset of monocytes (Figure 4B). UMAP analysis of the single-cell profile confirmed specific expression of *Zbtb46* and *Mafb* in the DC and IM clusters of control mice, further confirming our annotated myeloid clusters (Figure 3B). Interestingly, we observed a 2-fold increase in the percentage of *Mafb*-expressing cells having negligible expression of *Zbtb46* in cDC2 cluster 3 of *Adar1*$^{\Delta Cd11c}$ mice (Figure 3B). Further comparing UMAP and fold change in cell percentages of monocytes, macrophages, and DCs in the scRNA-seq profile from *Adar1*$^{\Delta Cd11c}$ and control mice (Figure 3A), we observed enrichment of Ly6C^{hi} monocytes cluster 1 (1.7-fold), Ly6C^{lo} monocyte cluster 2 (2.3-fold), and MHC class II+ IM population cluster 0 (2-fold) (Figure 3A). MHC class II− IM cluster 7 and AM cluster 4 were reduced by 2- and 4-fold in *Adar1*$^{\Delta Cd11c}$ mice, respectively (Figure 3A). As we enriched for AMs, the frequency of AM cluster 4 does not correlate with actual population frequencies as shown by flow cytometry. However, consistent with our flow cytometry observation, we saw a striking reduction in the cDC1 cluster 6, whereas the cDC2 cluster 3 was only modestly reduced (Figure 3A). In response to Toll-like receptor and type 1 IFN signaling, lung cDC2s can acquire expression of IRF8 and Fc receptor CD64, features shared with cDC1s and macrophages, respectively.[14] Since our BTM analysis showed upregulation of an ISG signature and our flow cytometry data showed upregulation of CD64 expression on APCs from lungs of *Adar1*$^{\Delta Cd11c}$ mice, we asked about the impact of ADAR1 deficiency on cDC2 heterogeneity. To this end, we re-embedded clusters representing cDC2s, cDC1s, and CCR7+ activated DCs (3, 6, and 8, respectively) and separated them into subclusters (Figure 3C). Next, we analyzed the expression of macrophage-specific Fc receptor CD64 and cDC1 transcription factor IRF8 in DC clusters. Single-cell UMAP analysis showed upregulation of CD64 in cDC2 cluster 0 in ADAR$^{\Delta Cd11c}$ mice (Figure 3D). We next assessed the expression of transcription factor *Irf8* in the cDC2 population in cluster 0 and observed the cDC2 population co-expressing *Irf8* and *CD64*, suggesting that cDC2s in *Adar1*$^{\Delta Cd11c}$ mice may represent a heterogeneous population of classical and inflammatory DC-like cells[14] (Figure 3D). Furthermore, analyses of gene signatures of cDC2 cluster 0 from ADAR$^{\Delta Cd11c}$ mice showed the upregulation of genes such as *Ifi205*, *Iy6a*, *Ifit3*, *Cxcl10*, *Ifit1*, *Ccl5*, *Cd7*, *Ntfc3*, *Cxcl9*, and *Gm4951*, observed to be expressed by inflammatory DCs in lungs (Figure 3E).[14] Next, we set out our focus to study the impact of ADAR1 deficiency on spleen APCs. To this end, we compared UMAP single-cell profiles of monocyte, macrophage, and DC clusters in *Adar1*$^{\Delta Cd11c}$ and control mice. UMAP and graph-based clusters segregated splenic monocytes into Ly6c+ monocytes (cluster 7) and Ly6c− monocytes (cluster 6) (Figure S2A). Splenic macrophages were separated into CD68+ macrophages (cluster 0), CD163+ red pulp macrophages (cluster 4), Marco+ marginal zone (MZ) macrophages (cluster 8), and Retn+ alternatively activated macrophages (cluster 10) (Figure S2A). DCs in the spleen were segregated into pDC cluster_5, cDC1 (cluster 2 and cluster_12), cDC2_A (cluster 1), cDC2_B (cluster 3), and mature regulatory DCs (mregDCs; cluster 11)[15,16] (Figure S2A). Concordant with our flow cytometry data, we observed reduced frequency of cDC1s and cDC2s (cDC2_A, cDC2B) by 1.4- and 2.3-fold, respectively (Figure S2A). Splenic macrophage and plasmacytoid DC (pDC) frequencies in *Adar1*$^{\Delta Cd11c}$ mice were comparable to control, whereas Ly6C− (cluster 6) and Ly6c+ monocyte (cluster 7) frequencies were increased (Figure S2A). As in the lung, we also analyzed the phenotype of splenic cDC2s in *Adar1*$^{\Delta Cd11c}$ mice by looking at the expression of *CD64* and

Figure 2. ADAR1 ablation in CD11c+ APCs has a global effect on transcriptional landscape of the immune system in the lung

Single-cell 10x RNA-seq analysis of lung immune population from *Adar1*$^{\Delta Cd11c}$ and control mice.

(A) Schematic overview of the experiment. Single-cell suspensions were stained with a panel of cell surface marker antibodies. Sorted T cells, alveolar macrophages (AMs), and CD11c+SiglecF− cells, and other immune cells were pooled at a ratio 15:15:5:65, respectively, and subjected to 10x single-cell RNA-seq.

(B) Annotated UMAP showing single-cell RNA-seq analysis of lung CD45$^+$ cell pooled from *Adar1*$^{\Delta Cd11c}$ and control mice.

(C) Bar plot showing number of DEGs between *Adar1*$^{\Delta Cd11c}$ and control mice in each cluster.

(D) BTMs significantly enriched (false discovery rate [FDR] < 0.001) in *Adar1*$^{\Delta Cd11c}$ compared with control mice. Overrepresentation analysis of the genes from (C) was used to determine significance.

(E) Heatmap showing top interferon-stimulated genes (ISGs) significantly enriched in *Adar1*$^{\Delta Cd11c}$ mice.

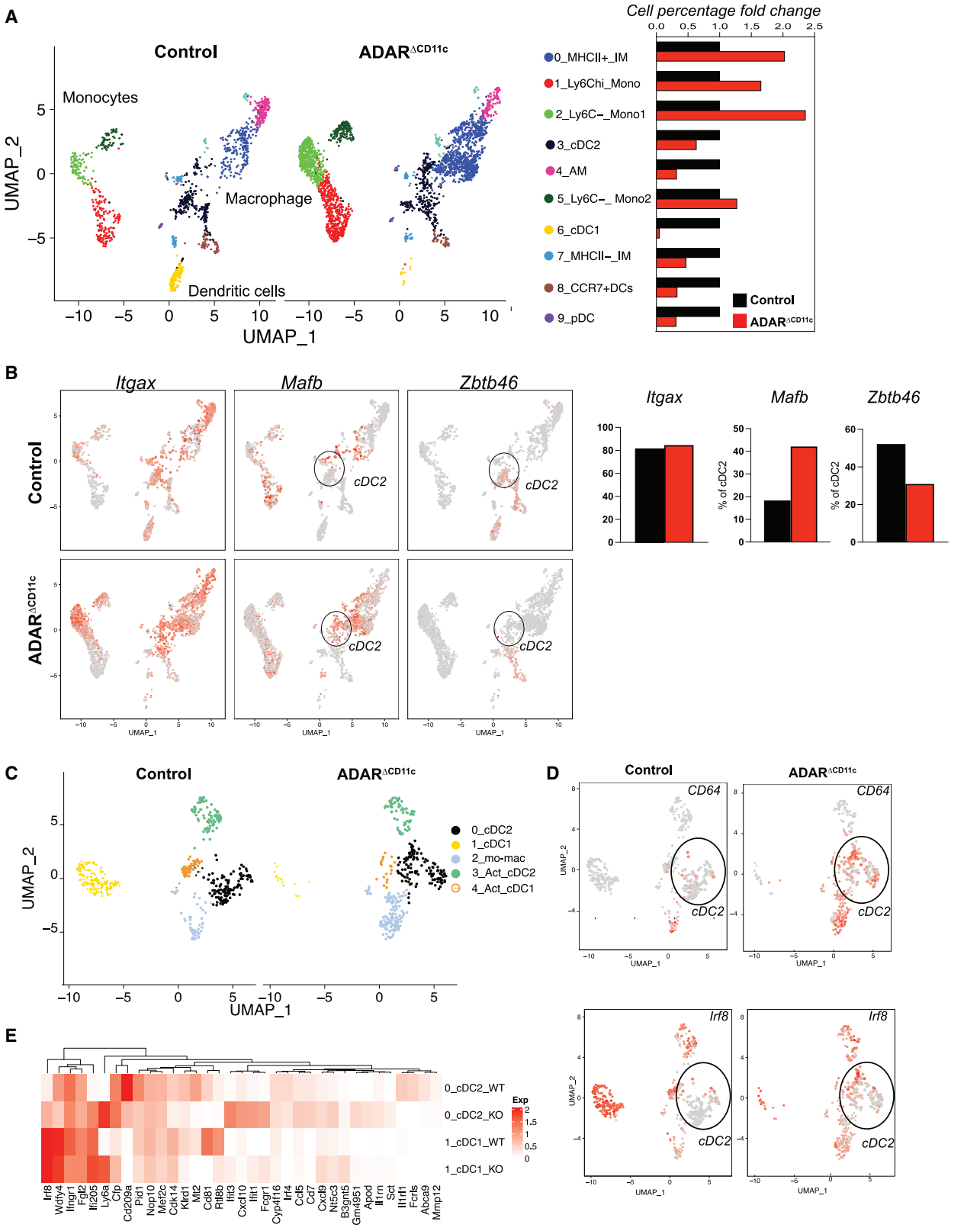

(legend on next page)

Irf8 in single-cell profiles of splenic DC clusters (Figures S2B and S2C). Interestingly single-cell UMAP analysis also showed upregulation of *CD64* and *Irf8* in spleen cDC2s (Figures S2C and S2D). Furthermore, analysis of signature genes such as *Ifi205*, *Ifi205*, *Ly6a*, *Ifit3*, *Cxcl10*, *Ifit1*, *Ccl5*, *Cd7*, *Ntfc3*, *Cxcl9*, *and Gm4951* expressed by inf-DCs were also found upregulated in splenic cDC2s of *Adar1*$^{\Delta Cd11c}$ mice (Figure S2D).[14] Thus, we conclude that ADAR1 ablation in CD11c+ cells affected myeloid cell homeostasis and skewed the ratio of cDC2s to inflammatory DC.

ADAR1 ablation in CD11c+ cells promotes T cell activation in the lung

cDCs link innate and adaptive immunity by recognizing PAMPs and presenting antigen to T cells. Given the role of cDCs in priming T cell responses, we next sought to better understand the effect of Adar1 ablation in APCs on T cells *in vivo*. Flow cytometry analysis of lung and spleen T cells revealed a significant increase in the proportion of CD62L−CD44+ effector memory (EM) cells among both CD4+ and CD8+ T cells in *Adar1*$^{\Delta Cd11c}$ mice, unique to the lung (Figures 4A, 4B, S3A, and S3B). EM T cells can establish residency within tissue to become TRMs. Given the skewing of lung T cells toward EM in in *Adar1*$^{\Delta Cd11c}$ mice, we looked within the EM subset at the expression of markers involved in tissue retention: CD69 and CD103. We observed a substantial increase in CD69+ and CD69+CD103+ EM T cells among both lung CD4+ and CD8+ T cells in *Adar1*$^{\Delta Cd11c}$ mice (Figures 4C and 4D), along with a modest but significant increase in CD103+ and CD69+CD103+ CD4+ EM T cells in the spleen (Figures S3C and S3D). Thus, despite altered APC homeostasis, naive *Adar1*$^{\Delta Cd11c}$ mice show an increase in lung EM CD4+ and CD8+ T cells that express markers associated with tissue residency *in vivo*.

Next, to confirm our flow cytometry analysis of T cell subsets, we combined all lung and spleen T cell clusters separately from each organ and re-clustered. scRNA-seq analysis of T cells in spleen and lung further corroborated the decrease in naive CD4+ and CD8+ T cells in favor of EM expansion in the lung (Figure 4E). In addition to ISG upregulation, analysis of DEGs within the EM clusters revealed downregulation of genes involved in T cell re-circulation: *S1pr1*, *Ccr7*, and *Klf2* (Figure 4F). Thus, consistent with flow cytometry analysis, scRNA-seq analysis of lung T cell subsets in *Adar1*$^{\Delta Cd11c}$ mice suggest that ADAR1 deletion in APCs promotes accumulation of CD4+ and CD8+ EM T cells that bear markers associated with tissue retention.

IFNAR1 blockade restores *Adar1*$^{\Delta Cd11c}$ defect in the spleen

Type I IFN signaling in DCs is critical for their development and function.[17–19] However, hyperactive type 1 IFN signaling in DCs can also be detrimental to their development and function.[20–23] Further, regulation of IFNAR1 signaling by transcription factor IRF2 has been demonstrated to be critical for homeostatic development of cDC2s in the spleen.[24,25] Given multiple lines of evidence pointing toward robust ISG induction in Adar1$^{\Delta Cd11c}$ APCs, we sought to determine the effect of type I IFN signaling on the APC defect in *Adar1*$^{\Delta Cd11c}$ mice. To this end, we repeatedly treated *Adar1*$^{\Delta Cd11c}$ mice with a high dose of α-IFNAR1 antibody or isotype control and assessed the impact of the treatment on lymphoid (spleen) and non-lymphoid (lung) tissue APCs (Figure 5A). α-IFNAR1 treatment of *Adar1*$^{\Delta Cd11c}$ mice restored total splenic MHC class II+CD11c+ DC frequencies to levels seen in controls due to an increase in both CD8α+ cDC1s and CD11b+ cDC2s (Figure 5B). Similarly, lung CD103+ cDC1s were restored to normal levels, while CD11b+ cDC2 frequencies were augmented relative to controls (Figure 5C). We next examined the expression of CD24 and CD64 within DCs and found that α-IFNAR1 treatment was not sufficient to reverse the skewing of the lung MHC class II+CD11c+ DC population toward the monocyte/macrophage CD24−CD64+ phenotype (Figure 5D). Further, lung AMs remained largely refractory to α-IFNAR1 treatment (Figure 5E). Thus, we concluded that IFNAR1 signaling in *Adar1*$^{\Delta Cd11c}$ APCs contributes to distinct tissue- and cell-specific phenotypes.

ADAR1 ablation in CD11c^{+} cells imprints an antiviral signature in alveolar type 2 epithelial cells and promotes resistance to early SARS-CoV-2 infection

SARS-CoV-2, the causative virus of the COVID-19 pandemic, evades early immune response by interfering with type I IFN response. Mutations that limit type I IFN induction and autoantibodies targeting IFN are associated with severe cases of COVID-19. Given that the spontaneous inflammatory changes observed in naive *Adar1*$^{\Delta Cd11c}$ mice were most pronounced in the lungs, we sought to evaluate their functional consequences in the context of respiratory tract infection. We challenged *Adar1*$^{\Delta Cd11c}$ mice and controls with the B.1.351 strain of SARS-CoV-2 virus.[26] At 3 days post-infection (dpi), *Adar1*$^{\Delta Cd11c}$ mice showed significantly lower viral titers than controls, accompanied by lower weight loss over the course of infection (Figures 6A and 6B). Histological analysis of lungs revealed accumulation of immune cells arranged in lymphofollicular aggregates along the adventitial surface of blood vessels in both naive and infected Adar1$^{\Delta Cd11c}$ but not controls (Figure 6C). Thus, we conclude that ADAR1 ablation in APCs improves outcome in early SARS-CoV-2 infection.

Lung alveolar type 2 epithelial cells are the targets of SARS-CoV-2 infection.[27] Given our observation of enhanced protection against mouse adapted SARS-CoV-2 in *Adar1*$^{\Delta Cd11c}$ mice, we asked whether inflammation in the mouse model extends beyond CD45+ cells, thus priming an antiviral immune response. To address this question, we isolated CD45+ immune

Figure 3. ADAR1 ablation in CD11c+ APCs alters lung myeloid cell homeostasis and skews the ratio of inflammatory DCs

Single-cell 10x RNA-seq analysis of lung myeloid cell population from *Adar1*$^{\Delta Cd11c}$ and control mice.

(A) UMAP and bar plot showing single-cell RNA-seq profile of lung myeloid population in control and *Adar1*$^{\Delta Cd11c}$ mice.

(B) Expression of *Itgax*, *Mafb*, and *Zbtb46* in lung myeloid population of control and *Adar1*$^{\Delta Cd11c}$ mice.

(C) UMAP showing single-cell RNA-seq profile of cDC subclusters.

(D) UMAP showing expression of *Irf8* and *CD64* in single-cell profile of cDCs clusters.

(E) Heatmap of gene signatures of inflammatory DCs in different cDC clusters.

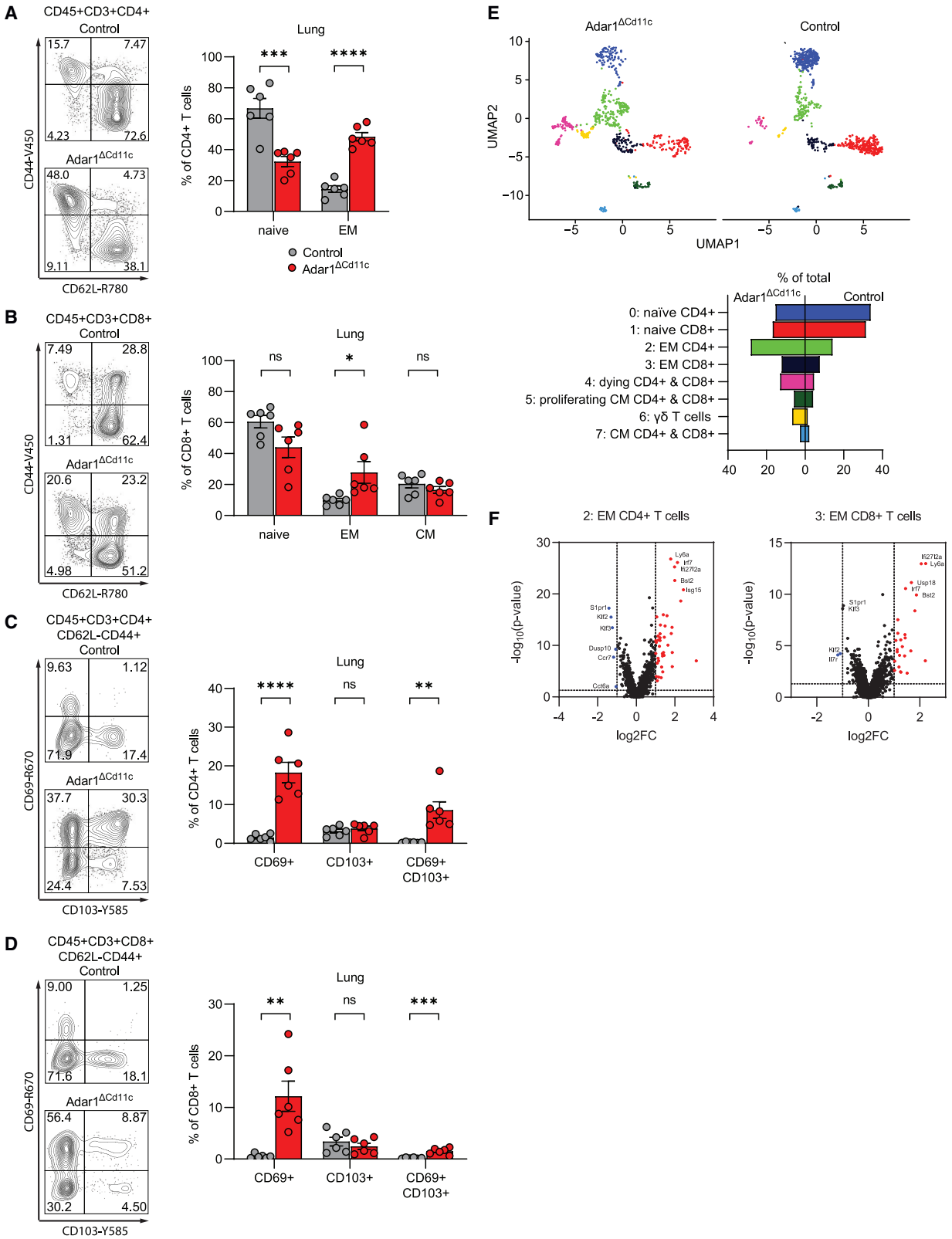

(legend on next page)

cells, EpCAM+ epithelial cells, and CD31+ endothelial cells from the lungs of naive *Adar1*$^{\Delta Cd11c}$ mice and controls and performed bulk RNA-seq (Figure 6D). Reactome pathway analysis revealed upregulation of inflammatory pathways present across immune, endothelial, and epithelial cells (Figure 6E). These pathways include genes known to be involved in antiviral defense, including RIG-I and MDA5, which are known to be responsible for sensing of SARS-CoV-2, providing a possible explanation for enhanced protection. We conclude that ADAR1 ablation in APCs imparts an inflammatory signature that extends beyond CD11c+ cells, thus priming the lungs for enhanced early antiviral protection.

DISCUSSION

Our current study demonstrates that conditional ablation of ADAR1 in CD11c+ cells broadly affects the homeostasis of the immune system. *Adar1*$^{\Delta Cd11c}$ mice have reduced frequency of AMs and cDCs. Mouse cDCs are classified into two functionally distinct lineages: CD8α+/CD103+ cDC1 and CD11b+ cDC2 lineages.[28,29] *Adar1*$^{\Delta Cd11c}$ mice showed a reduced frequency of cDC1s in the lung and spleen, whereas CD11b+ cDC2 frequencies were only reduced in the spleen. CD11b+ cDC2s classically defined in steady state as CD11c^{hi}MHCII^{hi}CD11b+ cells in mouse lungs represent a heterogeneous population comprising of CD24+CD11b+ cDC2s and CD64+CD11b+ monocyte-derived cells.[30] We further characterize the CD11b+ cDC2 population in lung of *Adar1*$^{\Delta Cd11c}$ mice by analyzing the expression of cDC-specific maker CD24 and macrophage-specific marker CD64 and demonstrated skewed CD11b^{+}cDC2 homeostasis toward CD64^{+}CD24^{lo}CD11b^{+} cDC2-like cells. These results are further supported by our scRNA-seq analysis, where we observed an increase in the frequency of CD64-expressing monocytes, monocyte-derived MHC class II+ IMs, and inflammatory DCs in lungs of *Adar1*$^{\Delta Cd11c}$ mice,[14,31] a similar phenotype to what we have previously observed in mice in which mTOR is deleted in CD11c+ APCs.[32] Single-cell analysis of the spleen also showed a similar trend of reduced frequency of cDCs and skewed cDC2 population toward inflammatory DC-like cells.[14] Our observations are consistent with the prior report of the effect of ADAR1 ablation on cDC1 and AM homeostasis.[6] The report also showed a significant reduction in the splenic CD11b+ cDC2 population, which was unaffected in the lungs of *Adar1*$^{\Delta Cd11c}$ mice. In our study, we provide evidence that the CD11b+ cDC2 subtype is also affected in the lung of *Adar1*$^{\Delta Cd11c}$ mice and is skewed toward inf-cDC2-like cells.[14]

In-depth analysis of the transcriptional profile of immune cells in *Adar1*$^{\Delta Cd11c}$ mice showed strong upregulation of antiviral gene signature in cDCs and AMs.[9] These results are consistent with findings from several groups based on the central role of ADAR1 in regulating chronic IFN response by preventing innate sensing of self-dsRNA by MDA5 and Z-DNA-binding protein 1 (ZBP1).[1,2,33–36] Interestingly, antiviral gene signatures are also induced in CD11c bystander cells, including other cells of the innate and adaptive immune system, as well as lung epithelial and endothelial cells, leading to the development of a global antiviral state in the lung. In addition to changes in steady state, we observe that ADAR1 ablation in APCs improves outcome in early SARS-CoV-2 infection. This enhanced protection can be explained by increased immune infiltration in the lung and ISGs in the epithelial cells that are targets of infection. Mice with mutations in the Zα domain of ADAR1, which show global spontaneous ISG induction, also exhibit enhanced capacity to clear encephalomyocarditis virus (ECMV) and influenza A virus.[37,38] Given the APC defects, it remains a question whether *Adar1*$^{-\Delta Cd11c}$ mice would continue to fare better in later stages of infection and whether they would be able to mount antigen-specific T cell and humoral responses that would confer protection against repeat viral exposure. However, the observation of early lower viral titers in *Adar1*$^{\Delta Cd11c}$ mice prompts the question of whether APC-specific ADAR1 dysregulation could be used as therapeutic in the context of infection and immunotherapy. Inhibition of ADAR1 releases a pool of self-dsRNAs to signal through MDA5. MDA5-overexpressing mice likewise show increased ISG induction and rapid clearance of vesicular stomatitis virus (VSV) infection despite any immune system defects.[39] In addition to the above result, we also provide evidence of a skewed cDC2 population toward inf-cDC2-like cells in *Adar1*$^{\Delta Cd11c}$ mice. This is supported by a study from Bosteels et al. where they observed IFN-dependent development of the inf-cDC2 population in lungs in the context of influenza infection and ongoing bone marrow-derived dendritic cell cultures when stimulated with an agonist of PRRs.

While IFNAR1 knockout (KO) is sufficient to rescue the inflammatory phenotype of a mouse with an AGS patient-derived mutation in the Z-alpha binding domain of ADAR1, it is not sufficient to rescue full ADAR1 KO.[34,40] Here, we demonstrate the unique dependence of the cDC defect in *Adar1*$^{\Delta Cd11c}$ mice on type I IFN signaling through the inhibition of IFNAR1 signaling. α-IFNAR1 treatment of *Adar1*$^{\Delta Cd11c}$ mice was sufficient to restore spleen and lung CD8α+/CD103+ cDC1s to normal frequencies. While the treatment led to normal CD11b+ cDC2 levels in the spleen, lung cDC2s were augmented while maintaining the CD24-CD64+ inflammatory phenotype. α-IFNAR1 was also not sufficient to restore the lung AM population in *Adar1*$^{\Delta Cd11c}$ within the treatment time frame. Thus, type I IFN signaling can be

Figure 4. ADAR1 ablation in APCs results leads to tissue-specific T cell activation

Lungs from naive *Adar1*$^{\Delta Cd11c}$ (red) or control (gray) mice were analyzed by flow cytometry for CD4+ and CD8+ T cell subsets.

(A and B) Frequency of lung naive (CD62L+CD44−), effector memory (EM; CD62L−CD44+), and central memory (CM; CD62L+CD44+) T cells as a percentage of the parent population, with representative contour plots.

(C and D) Frequency of CD69+ and CD103+ EM T cells in a percentage of all CD4+ or CD8+ T cells, with representative contour plots. Results are pooled from 2 independent experiments with n = 6 per group total, represented as mean ± SEM. Unpaired t test, ns, not significant, *p ≤ 0.05, **p ≤ 0.01, ***p ≤ 0.001, ****p ≤ 0.0001. Single-cell 10x RNA-seq analysis of lung T cell population from *Adar1*$^{\Delta Cd11c}$ and control mice.

(E) UMAP and bar plot showing single-cell RNA-seq profile of lung population and relative frequencies.

(F) Volcano plot of DEGs in EM populations.

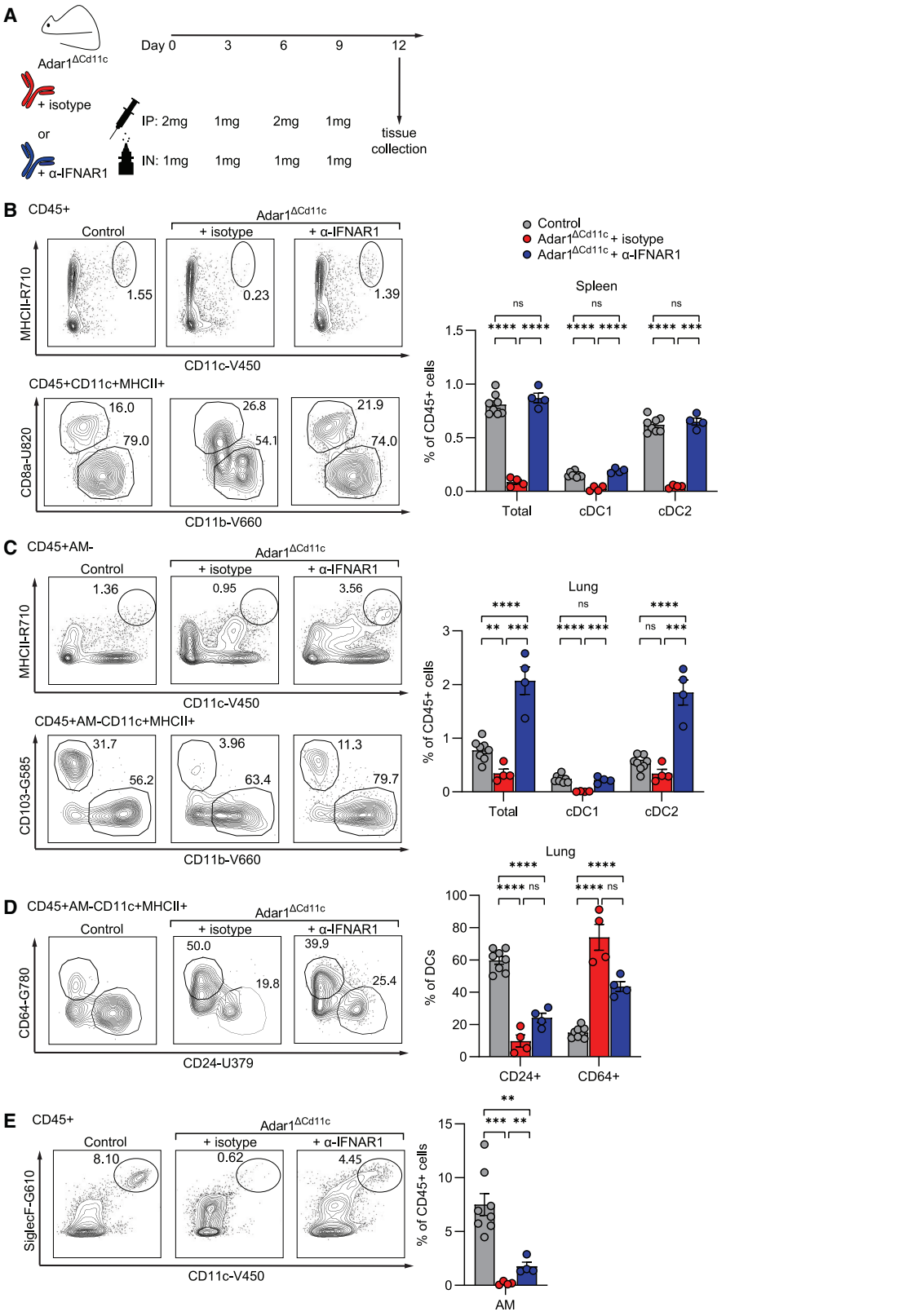

(legend on next page)

attributed to the reduction of DC frequencies seen in *Adar1*$^{\Delta Cd11c}$ mice but cannot completely explain the phenotypic skewing of lung cDC2s nor the absence of AMs. Inhibition of MDA5, mitochondrial antiviral signaling protein (MAVS) downstream of MDA5 signaling, or PKR activity in *Adar1*$^{\Delta Cd11c}$ mice could be used to further understand the mechanistic basis of perturbed homeostasis of DCs and AMs in *Adar1*$^{\Delta Cd11c}$ mice.[1,34] MAVS deletion in ADAR1 KO mice or ADAR1p150 isoform-deficient mice has previously been shown to promote an increase of CD11c+ DC levels in the spleens of 3- to 4-week-old mice compared with controls.[41]

In addition to myeloid cells, we also performed steady-state T cell analysis in *Adar1*$^{\Delta Cd11c}$ mice. cDCs prime T cell responses. While cDC1s (defective in *Adar1*$^{\Delta Cd11c}$ mice) are best among APCs at cross-presenting exogenous antigen on MHC class I to activate CD8+ T cells, inf-cDC2s (present in *Adar1*$^{\Delta Cd11c}$ mice) are capable of priming antigen-specific CD8+ and CD4+ T cell responses to a higher degree than cDC2s.[14] However, the previous report of an *in vitro* proliferation assay with lung DCs showed the decreased capacity of *Adar1*$^{\Delta Cd11c}$ cells to expand CD8+, but not CD4+, antigen-specific T cells. However, *in vivo,* we observed an increase in lung EM CD4+ and CD8+ T cells that express markers associated with activation and tissue residency CD69 and CD103, further corroborated by scRNA-seq analysis of the EM clusters, where we see downregulation of genes involved in T cell recirculation (*S1pr1*, *Ccr7*, *Klf2*). Given the *in vitro* report, the abundance of activated T cells in naive *Adar1*$^{\Delta Cd11c}$ mice raises the question of the process that gives rise to them and their antigen specificity for which further studies are needed.

Limitations of the study

The absence of ADAR1 in CD11c^{+} APCs alters the DC, AM, and T cell homeostasis. Our study suggests that ADAR1 ablation in APCs creates an antiviral state in the lungs and enhances early resistance of *Adar1*$^{\Delta Cd11c}$ mice to SARS-CoV-2 virus infection. Whether *Adar1*$^{\Delta Cd11c}$ mice would continue to have an advantage at later stages of the infection, when productive B and T cell responses are necessary, remains unknown. Further studies are also needed to determine if ADAR1 ablation in CD11c+ APCs confers protection against other respiratory pathogens, whether inhibition of ADAR1 in myeloid cells could promote antitumor immunity, and what consequences it has to tolerance to self-antigens.

STAR★METHODS

Detailed methods are provided in the online version of this paper and include the following:

- KEY RESOURCES TABLE
- RESOURCE AVAILABILITY
  - Lead contact
  - Material availability
  - Data and code availability
- EXPERIMENTAL MODEL AND SUBJECT DETAILS
  - Mice
- METHOD DETAILS
  - Tissue preparation for flow cytometry
  - Flow cytometry
  - Single cell RNA-seq analysis
  - IFNAR1 blockade
  - Lung bulk RNAseq
  - SARS-CoV-2 infection
  - Quantification of SARS-CoV-2 virus
  - Histology
- QUANTIFICATION AND STATISTICAL ANALYSIS

SUPPLEMENTAL INFORMATION

Supplemental information can be found online at https://doi.org/10.1016/j.celrep.2023.112038.

ACKNOWLEDGMENTS

We thank Danny Douek for sequencing and analysis of the B.1.351 variant (NIAID/NIH, Atlanta, GA, USA). The study was supported by NIH grants (R37 DK057665, R37 AI048638, U19 AI090023, and U19 AI057266 to R. Ahmed; U19 AI159840 to S. Foung; P51 OD011132 to M.S.S.), the Bill and Melinda Gates Foundation, and the Soffer Fund endowment and Open Philanthropy to B.P.

AUTHOR CONTRIBUTIONS

J.Z.A., R.V., and B.P. designed experiments, interpreted data, and wrote the manuscript. J.Z.A., R.V., F.W., and K.F. carried out experiments. E.V.V., Y.W., and M.T. maintained mouse colonies. S.G., T.H., and Q.L. performed RNA-seq analyses. J.G.V.-M. analyzed histological samples. C.R.W. provided mouse Adar1$^{fl/fl}$, R26^{YFP} mouse strain. S.S., M.S.S., and J.B.L. provided critical advice. All authors have read and approved the manuscript.

DECLARATION OF INTERESTS

B.P. has served or is serving on the External Immunology Network of GSK and is on the scientific advisory boards of Sanofi, Medicago, CircBio, and Boehringer-Ingelheim. M.S. has served or is serving as an external advisor for Moderna and Ocugen.

Received: September 8, 2022
Revised: November 25, 2022
Accepted: January 11, 2023

Figure 5. IFNAR1 blockade restores *Adar1*$^{\Delta Cd11c}$ defect in the spleen

Spleen and lungs from *Adar1*$^{\Delta Cd11c}$ mice treated with isotype control (red) or α-IFNAR1 (blue) were analyzed by flow cytometry and compared with untreated controls (gray).

(A) Timeline of antibody treatment.

(B) Total spleen MHC class II+CD11c+ DCs, CD8a+ cDC1s, and CD11b+ cDC2s, with representative contour plots.

(C) Frequency of lung MHC class II+CD11c+ DCs, CD103+ cDC1s, and CD11b+ cDC2s, with representative contour plots.

(D) Lung DCs were subset based on the expression of CD24 and CD64, with representative contour plots.

(E) SiglecF+CD11c+ AMs. Results are representative of 2 independent experiments with n = 3–8 per group each, represented as mean ± SEM. Unpaired t test, ns, not significant, *p ≤ 0.05, **p ≤ 0.01, ***p ≤ 0.001, ****p ≤ 0.0001.

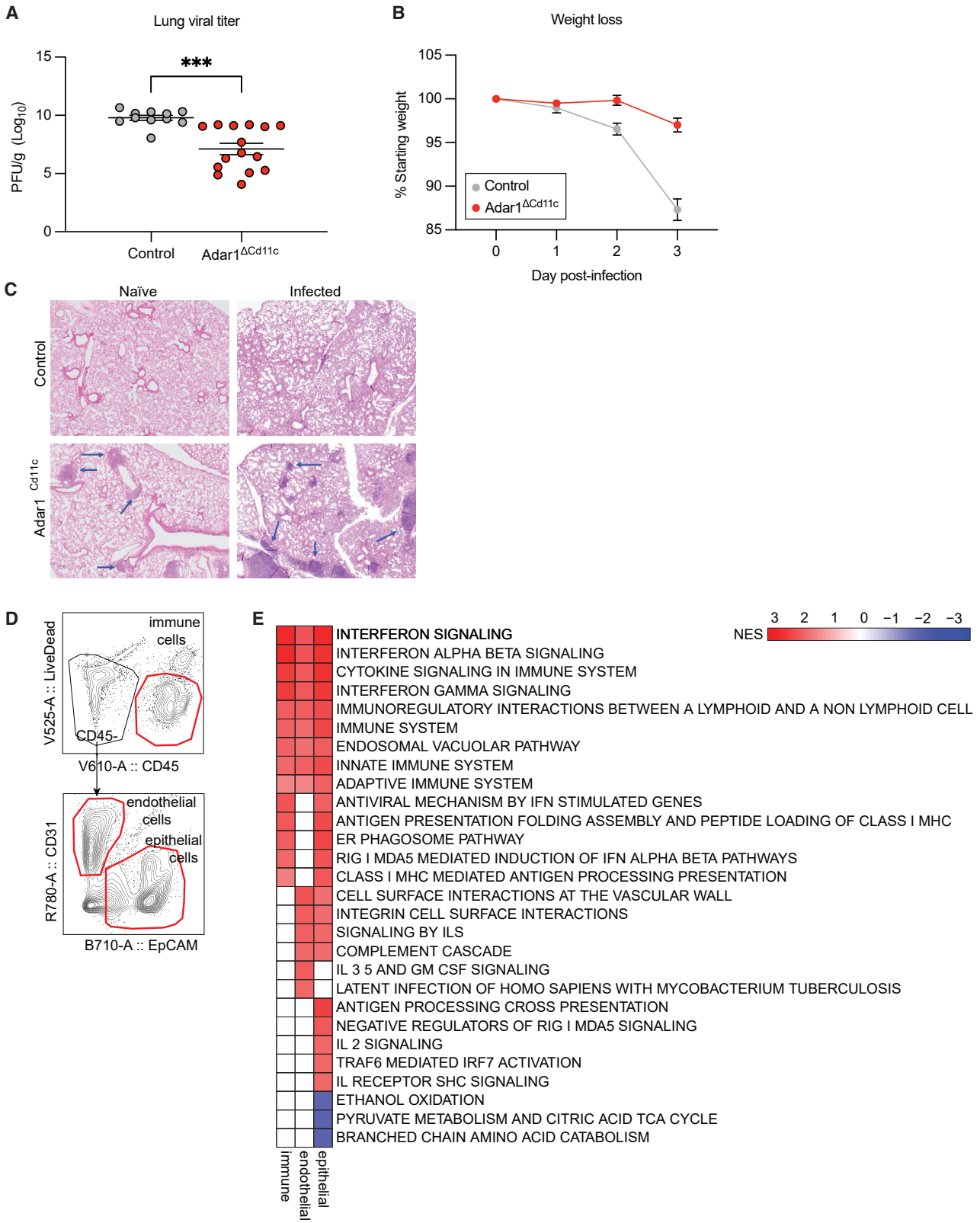

(legend on next page)

REFERENCES

1. Liddicoat, B.J., Piskol, R., Chalk, A.M., Ramaswami, G., Higuchi, M., Hartner, J.C., Li, J.B., Seeburg, P.H., and Walkley, C.R. (2015). RNA editing by ADAR1 prevents MDA5 sensing of endogenous dsRNA as nonself. Science *349*, 1115–1120. https://doi.org/10.1126/science.aac7049.
2. Chung, H., Calis, J.J.A., Wu, X., Sun, T., Yu, Y., Sarbanes, S.L., Dao Thi, V.L., Shilvock, A.R., Hoffmann, H.H., Rosenberg, B.R., and Rice, C.M. (2018). Human ADAR1 prevents endogenous RNA from triggering translational shutdown. Cell *172*, 811–824.e14. https://doi.org/10.1016/j.cell.2017.12.038.
3. Lamers, M.M., van den Hoogen, B.G., and Haagmans, B.L. (2019). ADAR1: "Editor-in-Chief" of cytoplasmic innate immunity. Front. Immunol. *10*, 1763. https://doi.org/10.3389/fimmu.2019.01763.
4. Rice, G.I., Kasher, P.R., Forte, G.M.A., Mannion, N.M., Greenwood, S.M., Szynkiewicz, M., Dickerson, J.E., Bhaskar, S.S., Zampini, M., Briggs, T.A., et al. (2012). Mutations in ADAR1 cause Aicardi-Goutieres syndrome associated with a type I interferon signature. Nat. Genet. *44*, 1243–1248. https://doi.org/10.1038/ng.2414.
5. Bhate, A., Sun, T., and Li, J.B. (2019). ADAR1: a new target for immuno-oncology therapy. Mol. Cell *73*, 866–868. https://doi.org/10.1016/j.molcel.2019.02.021.
6. Baal, N., Cunningham, S., Obermann, H.L., Thomas, J., Lippitsch, A., Dietert, K., Gruber, A.D., Kaufmann, A., Michel, G., Nist, A., et al. (2019). ADAR1 is required for dendritic cell subset homeostasis and alveolar macrophage function. J. Immunol. *202*, 1099–1111. https://doi.org/10.4049/jimmunol.1800269.
7. Heng, T.S.P., and Painter, M.W.; Immunological Genome Project Consortium (2008). The Immunological Genome Project: networks of gene expression in immune cells. Nat. Immunol. *9*, 1091–1094. https://doi.org/10.1038/ni1008-1091.
8. Li, S., Rouphael, N., Duraisingham, S., Romero-Steiner, S., Presnell, S., Davis, C., Schmidt, D.S., Johnson, S.E., Milton, A., Rajam, G., et al. (2014). Molecular signatures of antibody responses derived from a systems biology study of five human vaccines. Nat. Immunol. *15*, 195–204. https://doi.org/10.1038/ni.2789.
9. Schoggins, J.W., Wilson, S.J., Panis, M., Murphy, M.Y., Jones, C.T., Bieniasz, P., and Rice, C.M. (2011). A diverse range of gene products are effectors of the type I interferon antiviral response. Nature *472*, 481–485. https://doi.org/10.1038/nature09907.
10. Bar-On, L., and Jung, S. (2010). Defining in vivo dendritic cell functions using CD11c-DTR transgenic mice. Methods Mol. Biol. *595*, 429–442. https://doi.org/10.1007/978-1-60761-421-0_28.
11. Probst, H.C., Tschannen, K., Odermatt, B., Schwendener, R., Zinkernagel, R.M., and Van Den Broek, M. (2005). Histological analysis of CD11c-DTR/GFP mice after in vivo depletion of dendritic cells. Clin. Exp. Immunol. *141*, 398–404. https://doi.org/10.1111/j.1365-2249.2005.02868.x.
12. Satpathy, A.T., Wu, X., Albring, J.C., and Murphy, K.M. (2012). Re(de)fining the dendritic cell lineage. Nat. Immunol. *13*, 1145–1154. https://doi.org/10.1038/ni.2467.
13. Wu, X., Briseño, C.G., Durai, V., Albring, J.C., Haldar, M., Bagadia, P., Kim, K.W., Randolph, G.J., Murphy, T.L., and Murphy, K.M. (2016). Mafb lineage tracing to distinguish macrophages from other immune lineages reveals dual identity of Langerhans cells. J. Exp. Med. *213*, 2553–2565. https://doi.org/10.1084/jem.20160600.
14. Bosteels, C., Neyt, K., Vanheerswynghels, M., van Helden, M.J., Sichien, D., Debeuf, N., De Prijck, S., Bosteels, V., Vandamme, N., Martens, L., et al. (2020). Inflammatory type 2 cDCs acquire features of cDC1s and macrophages to orchestrate immunity to respiratory virus infection. Immunity *52*, 1039–1056.e9. https://doi.org/10.1016/j.immuni.2020.04.005.
15. Brown, C.C., Gudjonson, H., Pritykin, Y., Deep, D., Lavallée, V.P., Mendoza, A., Fromme, R., Mazutis, L., Ariyan, C., Leslie, C., et al. (2019). Transcriptional basis of mouse and human dendritic cell heterogeneity. Cell *179*, 846–863.e24. https://doi.org/10.1016/j.cell.2019.09.035.
16. Maier, B., Leader, A.M., Chen, S.T., Tung, N., Chang, C., LeBerichel, J., Chudnovskiy, A., Maskey, S., Walker, L., Finnigan, J.P., et al. (2020). A conserved dendritic-cell regulatory program limits antitumour immunity. Nature *580*, 257–262. https://doi.org/10.1038/s41586-020-2134-y.
17. Chen, Y.L., Chen, T.T., Pai, L.M., Wesoly, J., Bluyssen, H.A.R., and Lee, C.K. (2013). A type I IFN-Flt3 ligand axis augments plasmacytoid dendritic cell development from common lymphoid progenitors. J. Exp. Med. *210*, 2515–2522. https://doi.org/10.1084/jem.20130536.
18. Montoya, M., Schiavoni, G., Mattei, F., Gresser, I., Belardelli, F., Borrow, P., and Tough, D.F. (2002). Type I interferons produced by dendritic cells promote their phenotypic and functional activation. Blood *99*, 3263–3271. https://doi.org/10.1182/blood.v99.9.3263.
19. Simmons, D.P., Wearsch, P.A., Canaday, D.H., Meyerson, H.J., Liu, Y.C., Wang, Y., Boom, W.H., and Harding, C.V. (2012). Type I IFN drives a distinctive dendritic cell maturation phenotype that allows continued class II MHC synthesis and antigen processing. J. Immunol. *188*, 3116–3126. https://doi.org/10.4049/jimmunol.1101313.
20. Fuertes Marraco, S.A., Scott, C.L., Bouillet, P., Ives, A., Masina, S., Vremec, D., Jansen, E.S., O'Reilly, L.A., Schneider, P., Fasel, N., et al. (2011). Type I interferon drives dendritic cell apoptosis via multiple BH3-only proteins following activation by PolyIC in vivo. PLoS One *6*, e20189. https://doi.org/10.1371/journal.pone.0020189.
21. Teijaro, J.R., Ng, C., Lee, A.M., Sullivan, B.M., Sheehan, K.C.F., Welch, M., Schreiber, R.D., de la Torre, J.C., and Oldstone, M.B.A. (2013). Persistent LCMV infection is controlled by blockade of type I interferon signaling. Science *340*, 207–211. https://doi.org/10.1126/science.1235214.
22. Ng, C.T., Snell, L.M., Brooks, D.G., and Oldstone, M.B.A. (2013). Networking at the level of host immunity: immune cell interactions during persistent viral infections. Cell Host Microbe *13*, 652–664. https://doi.org/10.1016/j.chom.2013.05.014.
23. Wilson, E.B., Yamada, D.H., Elsaesser, H., Herskovitz, J., Deng, J., Cheng, G., Aronow, B.J., Karp, C.L., and Brooks, D.G. (2013). Blockade of chronic type I interferon signaling to control persistent LCMV infection. Science *340*, 202–207. https://doi.org/10.1126/science.1235208.
24. Honda, K., Mizutani, T., and Taniguchi, T. (2004). Negative regulation of IFN-alpha/beta signaling by IFN regulatory factor 2 for homeostatic development of dendritic cells. Proc. Natl. Acad. Sci. USA. *101*, 2416–2421. https://doi.org/10.1073/pnas.0307336101.
25. Ichikawa, E., Hida, S., Omatsu, Y., Shimoyama, S., Takahara, K., Miyagawa, S., Inaba, K., and Taki, S. (2004). Defective development of splenic and epidermal CD4+ dendritic cells in mice deficient for IFN regulatory

Figure 6. *Adar1*$^{\Delta Cd11c}$ mice promotes increased resistance to early SARS-CoV-2 infection

Adar1$^{\Delta Cd11c}$ (red) or control (gray) mice were infected intranasally with 10^6 PFUs of SARS-CoV-2 (B.1.351 strain) and sacrificed 3 days post-infection (dpi).

(A) Lung viral titer at 3 dpi measured by plaque assay.

(B) Weight loss dynamics. Representative results from 3 independent experiments with n = 15–18 per group, represented as mean ± SEM. Unpaired t test, *p ≤ 0.05, **p ≤ 0.01, ***p ≤ 0.001, ****p ≤ 0.0001.

(C) Representative H&E-stained sections of lung from naive and infected mice.

(D) Gating scheme for isolation of lung CD45+ immune cells, EpCAM+ epithelial cells, and CD31+ endothelial cells.

(E) Heatmap of differential Reactome pathways between *Adar1*$^{\Delta Cd11c}$ versus wild type (WT; FDR < 0.05, normalized enrichment score [NES] > 1.8) across lung cell types.

factor-2. Proc. Natl. Acad. Sci. USA. *101*, 3909–3914. https://doi.org/10.1073/pnas.0400610101.

26. Vanderheiden, A., Thomas, J., Soung, A.L., Davis-Gardner, M.E., Floyd, K., Jin, F., Cowan, D.A., Pellegrini, K., Shi, P.Y., Grakoui, A., et al. (2021). CCR2 signaling restricts SARS-CoV-2 infection. mBio *12*, e0274921. https://doi.org/10.1128/mBio.02749-21.
27. Ziegler, C.G.K., Allon, S.J., Nyquist, S.K., Mbano, I.M., Miao, V.N., Tzouanas, C.N., Cao, Y., Yousif, A.S., Bals, J., Hauser, B.M., et al. (2020). SARS-CoV-2 receptor ACE2 is an interferon-stimulated gene in human airway epithelial cells and is detected in specific cell subsets across tissues. Cell *181*, 1016–1035.e19. https://doi.org/10.1016/j.cell.2020.04.035.
28. Grajales-Reyes, G.E., Iwata, A., Albring, J., Wu, X., Tussiwand, R., Kc, W., Kretzer, N.M., Briseño, C.G., Durai, V., Bagadia, P., et al. (2015). Batf3 maintains autoactivation of Irf8 for commitment of a CD8alpha(+) conventional DC clonogenic progenitor. Nat. Immunol. *16*, 708–717. https://doi.org/10.1038/ni.3197.
29. Schlitzer, A., Sivakamasundari, V., Chen, J., Sumatoh, H.R.B., Schreuder, J., Lum, J., Malleret, B., Zhang, S., Larbi, A., Zolezzi, F., et al. (2015). Identification of cDC1- and cDC2-committed DC progenitors reveals early lineage priming at the common DC progenitor stage in the bone marrow. Nat. Immunol. *16*, 718–728. https://doi.org/10.1038/ni.3200.
30. Schlitzer, A., McGovern, N., Teo, P., Zelante, T., Atarashi, K., Low, D., Ho, A.W.S., See, P., Shin, A., Wasan, P.S., et al. (2013). IRF4 transcription factor-dependent CD11b+ dendritic cells in human and mouse control mucosal IL-17 cytokine responses. Immunity *38*, 970–983. https://doi.org/10.1016/j.immuni.2013.04.011.
31. Chakarov, S., Lim, H.Y., Tan, L., Lim, S.Y., See, P., Lum, J., Zhang, X.M., Foo, S., Nakamizo, S., Duan, K., et al. (2019). Two distinct interstitial macrophage populations coexist across tissues in specific subtissular niches. Science *363*, eaau0964. https://doi.org/10.1126/science.aau0964.
32. Sinclair, C., Bommakanti, G., Gardinassi, L., Loebbermann, J., Johnson, M.J., Hakimpour, P., Hagan, T., Benitez, L., Todor, A., Machiah, D., et al. (2017). mTOR regulates metabolic adaptation of APCs in the lung and controls the outcome of allergic inflammation. Science *357*, 1014–1021. https://doi.org/10.1126/science.aaj2155.
33. Ahmad, S., Mu, X., Yang, F., Greenwald, E., Park, J.W., Jacob, E., Zhang, C.Z., and Hur, S. (2018). Breaching self-tolerance to alu duplex RNA underlies MDA5-mediated inflammation. Cell *172*, 797–810.e13. https://doi.org/10.1016/j.cell.2017.12.016.
34. Mannion, N.M., Greenwood, S.M., Young, R., Cox, S., Brindle, J., Read, D., Nellåker, C., Vesely, C., Ponting, C.P., McLaughlin, P.J., et al. (2014). The RNA-editing enzyme ADAR1 controls innate immune responses to RNA. Cell Rep. *9*, 1482–1494. https://doi.org/10.1016/j.celrep.2014.10.041.
35. de Reuver, R., Verdonck, S., Dierick, E., Nemegeer, J., Hessmann, E., Ahmad, S., Jans, M., Blancke, G., Van Nieuwerburgh, F., Botzki, A., et al. (2022). ADAR1 prevents autoinflammation by suppressing spontaneous ZBP1 activation. Nature *607*, 784–789. https://doi.org/10.1038/s41586-022-04974-w.
36. Hubbard, N.W., Ames, J.M., Maurano, M., Chu, L.H., Somfleth, K.Y., Gokhale, N.S., Werner, M., Snyder, J.M., Lichauco, K., Savan, R., et al. (2022). ADAR1 mutation causes ZBP1-dependent immunopathology. Nature *607*, 769–775. https://doi.org/10.1038/s41586-022-04896-7.
37. de Reuver, R., Dierick, E., Wiernicki, B., Staes, K., Seys, L., De Meester, E., Muyldermans, T., Botzki, A., Lambrecht, B.N., Van Nieuwerburgh, F., et al. (2021). ADAR1 interaction with Z-RNA promotes editing of endogenous double-stranded RNA and prevents MDA5-dependent immune activation. Cell Rep. *36*, 109500. https://doi.org/10.1016/j.celrep.2021.109500.
38. Tang, Q., Rigby, R.E., Young, G.R., Hvidt, A.K., Davis, T., Tan, T.K., Bridgeman, A., Townsend, A.R., Kassiotis, G., and Rehwinkel, J. (2021). Adenosine-to-inosine editing of endogenous Z-form RNA by the deaminase ADAR1 prevents spontaneous MAVS-dependent type I interferon responses. Immunity *54*, 1961–1975.e5. https://doi.org/10.1016/j.immuni.2021.08.011.
39. Crampton, S.P., Deane, J.A., Feigenbaum, L., and Bolland, S. (2012). Ifih1 gene dose effect reveals MDA5-mediated chronic type I IFN gene signature, viral resistance, and accelerated autoimmunity. J. Immunol. *188*, 1451–1459. https://doi.org/10.4049/jimmunol.1102705.
40. Maurano, M., Snyder, J.M., Connelly, C., Henao-Mejia, J., Sidrauski, C., and Stetson, D.B. (2021). Protein kinase R and the integrated stress response drive immunopathology caused by mutations in the RNA deaminase ADAR1. Immunity *54*, 1948–1960.e5. https://doi.org/10.1016/j.immuni.2021.07.001.
41. Pestal, K., Funk, C.C., Snyder, J.M., Price, N.D., Treuting, P.M., and Stetson, D.B. (2015). Isoforms of RNA-editing enzyme ADAR1 independently control nucleic acid sensor MDA5-driven autoimmunity and multi-organ development. Immunity *43*, 933–944. https://doi.org/10.1016/j.immuni.2015.11.001.
42. Stuart, T., Butler, A., Hoffman, P., Hafemeister, C., Papalexi, E., Mauck, W.M., 3rd, Hao, Y., Stoeckius, M., Smibert, P., and Satija, R. (2019). Comprehensive integration of single-cell data. Cell *177*, 1888–1902.e21. https://doi.org/10.1016/j.cell.2019.05.031.
43. Zhang, X., Lan, Y., Xu, J., Quan, F., Zhao, E., Deng, C., Luo, T., Xu, L., Liao, G., Yan, M., et al. (2019). CellMarker: a manually curated resource of cell markers in human and mouse. Nucleic Acids Res. *47*, D721–D728. https://doi.org/10.1093/nar/gky900.
44. Yu, G., Wang, L.G., Han, Y., and He, Q.Y. (2012). clusterProfiler: an R package for comparing biological themes among gene clusters. OMICS *16*, 284–287. https://doi.org/10.1089/omi.2011.0118.
45. Nakano, H., Nakano, K., and Cook, D.N. (2018). Isolation and purification of epithelial and endothelial cells from mouse lung. Methods Mol. Biol. *1799*, 59–69. https://doi.org/10.1007/978-1-4939-7896-0_6.
46. Love, M.I., Huber, W., and Anders, S. (2014). Moderated estimation of fold change and dispersion for RNA-seq data with DESeq2. Genome Biol. *15*, 550. https://doi.org/10.1186/s13059-014-0550-8.

STAR★METHODS

KEY RESOURCES TABLE

REAGENT or RESOURCE	SOURCE	IDENTIFIER
Antibodies		
Rat anti-mouse CD16/32	BD Biosciences	Cat# 553142; RRID: AB_394657, Clone# 2.4G2
Rat anti-mouse CD45, Brilliant Violet 605	BioLegend	Cat# 103139; RRID:AB_2562341, Clone# 30-F11
Rat anti-mouse CD3, Brilliant Violet 785	BioLegend	Cat# 100231; RRID:AB_11218805, Clone# 17A2
Rat anti-mouse CD4, Brilliant Violet 650	BioLegend	Cat# 100545; RRID:AB_11126142, Clone# RM4-5
Rat anti-mouse CD8α, Brilliant Violet 711	BioLegend	Cat# 100747; RRID:AB_11219594, Clone# 53-6.7
Rat anti-mouse CD8α, BUV805	BD Biosciences	Cat# 612898; RRID:AB_2870186, Clone# 53-6.7
Rat anti-mouse CD62L, APC/Cy7	BioLegend	Cat# 104427; RRID: AB_830798, Clone# MEL-14
Rat anti-mouse CD44, Brilliant Violet 421	BioLegend	Cat# 103039; RRID: AB_10895752, Clone# IM7
Armenian hamster anti-mouse CD69, Alexa Fluor 647	BioLegend	Cat# 104517; RRID: AB_492848, Clone# H1.2F3
Armenian hamster anti-mouse CD103, PE	BioLegend	Cat# 121405; RRID: AB_535948, Clone# 2E7
Rat anti-mouse CD19, PerCP/Cy5.5	BioLegend	Cat#115533; RRID: AB_2259869, Clone# 6D5
Rat anti-mouse SiglecF, PE/Dazzle 595	BioLegend	Cat# 155529; RRID: AB_2890716, Clone# S17007L
Rat anti-mouse I-A/I-E (MHCII), Alexa Fluor 700	BioLegend	Cat# 107621; RRID: AB_493726, Clone# M5/114.15.2
Rat anti-mouse CD11c, Brilliant Violet 421	BioLegend	Cat# 117329; RRID: AB_10897814, Clone# N418
Rat anti-mouse CD11b, Brilliant Violet 650	BioLegend	Cat# 101239; RRID: AB_11125575, Clone# M1/70
Rat anti-mouse CD86, Alexa Fluor 647	BioLegend	Cat# 105019; RRID: AB_493465, Clone# GL-1
Rat anti-mouse CD24, BUV379	BD Biosciences	Cat# 744471; RRID: AB_2742259, Clone# M1/69
Mouse anti-mouse CD64, PE/Cy7	BioLegend	Cat# 139313; RRID: AB_2563903, Clone# X54-5/7.1
Rat anti-mouse Ly6C, Brilliant Violet 785	BioLegend	Cat# 128041; RRID: AB_2565852, Clone# HK1.4
Rat anti-mouse Ly6G, APC/Cy7	BioLegend	Cat# 127623; RRID: AB_10645331, Clone# 1A8
Rat anti-mouse CD31, APC/Fire750	BioLegend	Cat# 102433; RRID: AB_10645331, Clone# 390
Rat anti-mouse EpCAM, PerCP/Cy5.5	BioLegend	Cat# 118219; RRID: AB_2098647, Clone# G8.8
Mouse anti-mouse IFNAR1 (Ultra-LEAF purified)	BioLegend	Cat# 127324; RRID: AB_2629522, Clone# MAR1-5A3
Mouse IgG1 κ isotype control antibody (Ultra-LEAF purified)	BioLegend	Cat# 400198, Clone# MOPC-21
Deposited data		
scRNAseq	This paper	GEO: GSE222487
Bulk RNAseq	This paper	GEO: GSE222326
Experimental models: Organisms/strains		
Mouse: *Adar1*$^{fl/fl}$, *R26*^{YFP}	Dr. Carl Walkley (St Vincent's Institute, Melbourne, Australia)	MGI:3029789
Mouse: *CD11c*-Cre$^{+/-}$: B6.Cg-Tg(Itgax-cre)1-1Reiz/J	The Jackson Laboratory	RRID: IMSR_JAX:008,068
Software and algorithms		
FlowJo	BD Biosciences	Version 10.8.1
GraphPad Prism 9	Dotmatics	Version 9.4.0
Code for bulk RNA-seq analysis	This paper	Zenodo: https://doi.org/10.5281/zenodo.7519211

RESOURCE AVAILABILITY

Lead contact

Further information and requests for resources and reagents should be directed to and will be fulfilled by the lead contact, Bali Pulendran (bpulend@stanford.edu).

Material availability

All unique mouse lines generated in this study are available from the lead contact without restriction.

Data and code availability

Bulk and single-cell RNAseq data reported in this study have been deposited in the GEO and are publicly available as of the date of publication. Accession numbers are listed in the key resources table. All original code has been deposited at Zenodo and is publicly available as of the date of publication. DOIs are listed in the key resources table. Any additional information required to reanalyze the data reported in this paper is available from the lead contact upon request.

EXPERIMENTAL MODEL AND SUBJECT DETAILS

Mice

Mice were bred and housed at the Stanford Research Animal Facility (Stanford University, Stanford, CA), under specific pathogen-free conditions. Experimental mice of both sexes were used between 6 and 20 weeks of age. All animal protocols were reviewed and approved by the Stanford University Institutional Animal Care and Use Committee (APLAC-32681). Mouse genotyping was confirmed using PCR analysis of ear biopsies. *Adar1*$^{fl/fl}$, *R26*^{YFP} mice were kindly provided by Dr. Carl Walkley (St Vincent's Institute, Melbourne, Australia) and crossed with CD11c-Cre$^{+/-}$ mice to generate *Cd11c*-Cre$^{+/-}$ *Adar1*$^{fl/fl}$ *R26*^{YFP} mice (*Adar1*$^{\Delta Cd11c}$). Sex-matched *Cd11c*-Cre$^{-/-}$*Adar1*$^{fl/fl}$ *R26*^{YFP} littermates or age- and sex-matched *Cd11c*-Cre$^{+/-}$ mice were used as controls. For infection studies mice were transferred to Emory University (Atlanta, GA). All animal protocols were reviewed and approved by the Emory University Institutional Animal Care and Use Committee (PROTO201700309).

METHOD DETAILS

Tissue preparation for flow cytometry

Euthanized mice were perfused with 5mL PBS injected through the right ventricle of the heart. Lungs were cut with scissors and digested in 1 mg/mL type 4 collagenase with DNAse I (Sigma) dissolved in HBSS with 2% FBS. Digestion was performed for 45 min at 37°C shaking at 200rpm, and reactions were stopped with addition of EDTA. Cells were passed through a 70μm cell strainer. Red blood cells were lysed with 1mL ACK lysing buffer (Lonza). T cells were purified using a 30%/70% Percoll gradient (GE Healthcare).

Spleens were cut with scissors and digested in 1 mg/mL collagenase type 4 (Worthington Biochemical Corporation) dissolved in HBSS with 2% FBS. Digestion was performed for 30 min at 37°C and reactions stopped with addition of EDTA. Cells were passed through a 70μm cell strainer. Red blood cells were lysed with 1mL ACK lysing buffer (Lonza).

Flow cytometry

Single cell suspensions were stained for viability with Ghost Dye Violet 510 (Tonbo Biosciences). Washed cells were incubated with Fc receptor blocking antibody anti-CD16/32 (2.4G2) and stained with fluorochrome conjugated antibodies purchased from BioLegend or BD Biosciensces against: CD45 (30-F11), CD3 (17A2), CD4 (RM4-5), CD8α (53-6.7), CD62L (MEL-14), CD44 (IM7), CD69 (H1.2F3), CD103 (2E7), CD19 (6D5), SiglecF (S17007L), MHCII (M5/114.15.2), CD11c (N418), CD11b (M1/70), CD86 (GL-1), CD24 (M1/69), CD64 (X54-5/7.1), Ly6C (HK1.4), Ly6G (1A8), CD31(390), EpCAM (G8.8). Samples were fixed, data acquired on BD LSRII flow cytometer at the Stanford Shared FACS Facility (obtained using NIH S10 Shared Instrument Grant, S10RR027431-01), and analyzed using FlowJo software (BD Biosciences).

Single cell RNA-seq analysis

Single cell RNAseq data of lung and spleen immune cell populations were analyzed using Seurat.[42] Cells containing <200 RNA features were removed. Filtered RNA counts were normalized using LogNormalize method implemented in Seurat with a scale factor of 10,000. FindIntegrationAnchors and IntegrateData function in Seurat were used to integrate all the samples. We selected 30 principal components for clustering and UMAP projection. Clusters were identified using SNN graph and original Louvain algorithm with a resolution of 0.5, resulting in 23 clusters in the lung and 22 clusters in the spleen. FindAllMarkers function in Seurat and Cell Markers database enrichment using clusterProfiler were used to identify cluster marker genes (p value $\leq$0.01, log fold change (LFC) $\geq$ 0.25) and cell type enrichments for initial cluster annotations.[43,44] Clusters were further checked and annotated manually using ImmGen database. FindMarkers function in Seurat and BTMs enrichment using hypergeometric distribution were used to identify differentially regulated genes (p value $\leq$0.05, LFC $\geq$0.15) and their functional annotations. Myeloid cells were analyzed thoroughly by selecting macrophage and dendritic cells (DCs) (clusters 1, 2, 5, 7, 13, 14, 19 and 22 in lungs and clusters 2, 5, 10, 11, 13, 16, 17 and 19 in spleen) and clustering again with a resolution of 0.25 and 0.4 to get 11 and 14 clusters in lung and spleen, respectively. DCs (clusters 3, 6, and 8) in lung were selected from myeloid UMAP and clustered again with resolution of 0.25 to get 5 clusters for deeper cell population analysis. Similarly, T cells (clusters 8, 9, 11 and 20 in lung and clusters 1, 3, 7 and 12 in spleen) were further analyzed by running the Seurat pipeline with resolution of 0.25 and 0.4, respectively, to get 8 clusters in both lung and spleen.

IFNAR1 blockade

Mice were administered multiple does of purified anti-IFNAR1 (MAR1-5A3) or mouse IgG1 κ isotype control antibody intraperitoneally (day 0, 6: 2mg; day 3, 9: 1mg) and intranasally (day 0, 3, 6, and 8: 1mg) under isoflurane anesthesia.

Lung bulk RNAseq

Lungs were collected, digested, processed into single cell suspensions, and stained with fluorochrome conjugated antibodies as described in a protocol by Nakano et al. 2018.[45] Immune cells (CD45+), epithelial cells (CD45-EpCAM+CD31-), and endothelial cells (CD45-EpCAM-CD31+) were purified using the Aria II fluorescence activated cell sorter (BD Bioscience) and lysed in 350μL of Buffer RLT with β-ME (Qiagen). RNA was extracted using the RNeasy Mini kit (Qiagen) with on-column DNase digestion. RNAseq libraries were prepared using 6ng of RNA and the Kapa library preparation kit (Roche) and sequenced at 2x75bp on NextSeq (Illumina). Sequencing data was aligned to Mus Musculus Reference Genome (version GRCm38).

For analysis, gene-level counts were normalized using the DESeq2 package,[46] filtered to remove those with a median expression less than 32, and converted to log2. For use with Reactome pathways, mouse genes were converted to human homologs in the human reference genome (version GRCh38.p13), with expression for human genes with multiple mouse homologs computed via mean expression. Enrichment analysis was performed via the fgsea package, using genes ranked by $Adar1^{\Delta Cd11c}$ vs control FC in each cell type. All code was written in R (v4.1.2).

SARS-CoV-2 infection

The B.1.351 variant of SARS-CoV-2 was provided by Dr. Andy Pekosz (John Hopkins University, Baltimore, MD). Viral stocks were grown on VeroE6-TMPRSS2 cells and viral titers were determined by plaque assay on VeroE6-TMPRSS2. Cells were cultured in complete DMEM medium consisting of 1x DMEM (Corning Cellgro), 10% FBS, 25 mM HEPES Buffer (Corning Cellgro), 2 mM L-glutamine, 1mM sodium pyruvate, 1x non-essential amino acids, 1x antibiotics and Puromycin 10 mg/mL (# A11138-03). Mice were infected intranasally with 10^6 PFU SARS-CoV-2 (B.1.351 strain) under isoflurane anesthesia in an ABSL-3 facility. Mice were monitored daily for weight loss.

Quantification of SARS-CoV-2 virus

At 3 days post-infection, mice were euthanized via isoflurane overdose and lung tissue was collected in Omni-Bead Ruptor tubes filled with 1% FBS-HBSS. Tissue was homogenized in an Omni Bead Ruptor 24 (5.15 ms, 15 s). To perform plaque assays, 10-fold dilutions of viral supernatant in serum free DMEM (VWR, #45000-304) were overlaid on VeroE6-TMPRSS2-hACE2 cells monolayers and adsorbed for 1 h at 37°C. After adsorption, 0.5% immunodiffusion Agarose in 2X DMEM supplemented with 5% FBS (Atlanta Biologics) and 1X sodium bicarbonate was overlaid, and cultures were incubated for 48 h at 37°C. Agarose plugs were removed, cells fixed with 4% PBS-buffered paraformaldehyde for 15 min at room temperature and plaques were visualized using crystal violet staining (20% methanol in ddH2O).

Histology

Lungs were inflated with 10% neutral buffered formalin (NBF), immersion fixed in NBF for 72 h, routinely processed, and embedded to yield formalin-fixed paraffin-embedded (FFPE) tissue blocks. FFPE samples were sectioned at 5μm and routinely stained with hematoxylin and eosin. Tissue sections were visualized with an Olympus BX43 brightfield microscope, and images captured using an Olympus DP27 camera and the Olympus cellSens software. Images were captured at 4× magnification.

QUANTIFICATION AND STATISTICAL ANALYSIS

Analyses were performed using GraphPad Prism 9 software (Dotmatics). Statistical differences between groups were calculated using the unpaired t test, with significance denoted as: ns = not significant, *$p \leq 0.05$, **$p \leq 0.01$, ***$p \leq 0.001$, ****$p \leq 0.0001$.